

# High-density, high-mobility ultrathin spin-polarized two-dimensional electron gas at the polar/polar LaVO<sub>3</sub>/KTaO<sub>3</sub> interface: Insights from first-principles calculations

Arpan Das<sup>1,2,\*</sup>

<sup>1</sup>Theoretical Sciences Unit, Jawaharlal Nehru Centre for Advanced Scientific Research, Jakkur, Bangalore 560064, India

<sup>2</sup>Department of Science and Humanities, Audisankara (Deemed to be University), Gudur 524101, India

(Dated: June 4, 2026)

The emergence of high-mobility two-dimensional electron gases (2DEGs) at oxide interfaces provides a fertile platform for exploring emergent quantum phenomena and next-generation oxide electronics. Here, using first-principles density functional theory (DFT) calculations, we uncover the microscopic origin of the 2DEG formed at the interface between the band insulator KTaO<sub>3</sub> (KTO) and the Mott insulator LaVO<sub>3</sub> (LVO). Despite both constituents being insulating in bulk, the LVO/KTO heterostructure develops robust metallicity at the interface, in agreement with experimental observations. Our calculations reveal that this metallic state arises from an electronic reconstruction mechanism driven by the polar discontinuity across the interface. To avert the polar catastrophe on both the polar LVO film and the polar KTO substrate, electrons are transferred from the outer surfaces toward the interface, resulting in hole accumulation in the surface VO<sub>2</sub> layer and electron accumulation in the interfacial TaO<sub>2</sub> layer. This charge redistribution stabilizes a highly confined and spin-polarized 2DEG localized at the interface. The electronic states forming the 2DEG are predominantly derived from the interfacial Ta  $5d_{xy}$  orbitals, enforcing carrier motion strictly within the interfacial plane. Remarkably, the spin-up parabolic band hosting the 2DEG exhibits an exceptionally small effective mass – substantially lower than that of the prototypical LaAlO<sub>3</sub>/SrTiO<sub>3</sub> interface – indicating the potential for significantly enhanced carrier mobility. Furthermore, the calculated interfacial electron density exceeds that of LaAlO<sub>3</sub>/SrTiO<sub>3</sub> by nearly an order of magnitude, consistent with experimental measurement. These findings identify the LVO/KTO heterostructure as a compelling platform for realizing high-density, high-mobility spin-polarized 2DEGs and open new avenues for engineering correlated oxide interfaces for quantum electronic applications.

## I. INTRODUCTION

A two-dimensional electron gas (2DEG) refers to a system of free electrons confined within a two-dimensional plane, typically at the interface between two semiconductors or two insulators. In such systems, electrons are free to move in two dimensions along the interface, e.g., in the  $xy$ -plane, but are strongly confined in the third dimension perpendicular to the interface, i.e., along the  $z$ -axis. One of the most common realizations of 2DEGs occurs at interfaces in metal–oxide–semiconductor field-effect transistors (MOSFETs). When two or more oxides are combined to form heterostructures, a rich variety of emergent phenomena can arise in addition to the formation of a 2DEG, including ferroelectricity, half-metallicity, multiferroicity, high-temperature superconductivity, optical and electrical effects, the quantum Hall effect, coexistence of ferromagnetism and superconductivity, photoconductivity, resistance switching, Shubnikov–de Haas oscillations, quantum oscillations in conductivity, and colossal magnetoresistance.<sup>1–21</sup> Such oxide heterostructures can be fabricated experimentally using thin-film deposition techniques such as pulsed laser deposition and molecular beam epitaxy.<sup>22,23</sup> In 2004, Ohtomo and Hwang reported, for the first time, electronic conduction or a metallic phase at the interface between two insulating perovskites, LaAlO<sub>3</sub> and SrTiO<sub>3</sub>.<sup>24</sup> Since then,

the LaAlO<sub>3</sub>/SrTiO<sub>3</sub> interface, commonly referred to as LAO/STO, has become one of the most extensively studied oxide heterointerfaces over the past two decades.<sup>25–27</sup> The metallic phase is confined within a few nanometers of the interface,<sup>27</sup> and can therefore be treated as a 2DEG with a very high carrier density of  $\sim 10^{13}$  cm<sup>-2</sup> and high mobility of  $\sim 10^3$  cm<sup>2</sup> V<sup>-1</sup> s<sup>-1</sup>, making it highly attractive for nanoelectronic applications such as oxide field-effect transistors.<sup>14,28–30</sup>

A fundamental question arises: why does a metallic state emerge at the interface between two semiconductors or insulators? Several well-established mechanisms have been proposed for the formation of a 2DEG. (i) *Electronic reconstruction* driven by *polar catastrophe*.<sup>25</sup> In the polar/nonpolar LAO/STO interface, LAO consists of alternating charged planes (LaO)<sup>+1</sup> and (AlO<sub>2</sub>)<sup>-1</sup>, whereas STO is composed of neutral layers (SrO)<sup>0</sup> and (TiO<sub>2</sub>)<sup>0</sup>. This results in a finite polarization within the polar LAO film. When the polar LAO film is grown on the STO(001) substrate, a polarization discontinuity develops at the interface, leading to an increase in electrostatic potential with increasing film thickness. Consequently, a potential divergence, known as the *polar catastrophe*, arises and destabilizes the system. To avoid this divergence,  $\frac{1}{2}$  electron (per unit area of the interface) is transferred from the surface of the LAO film to the LAO/STO interface, thereby neutralizing the potential buildup. The migrated electrons accumulate at the interface and form the 2DEG. (ii) *Modulation doping*.<sup>31–33</sup> In this mechanism, band bending at the heterointerface, together with

\* arpandas9236@gmail.com

$n$ -type doping and electrostatic gating, shifts the Fermi level into the lower region of the conduction band minimum (CBM), leading to the formation of a 2DEG extending from the CBM up to the Fermi level. (iii) *Oxygen vacancies*.<sup>34–36</sup> An oxygen vacancy near the interface leaves behind two mobile electrons, which can contribute to the formation of a 2DEG. (iv) *Cation intermixing*.<sup>37–39</sup> For example, at the LAO/STO interface, intermixing of  $\text{Sr}^{2+}$  and  $\text{La}^{3+}$  cations can occur, introducing extra conduction electrons at the interface and thereby contributing to the formation of a 2DEG.

2DEGs can also emerge at nonpolar/nonpolar interfaces such as  $\text{CaZrO}_3/\text{SrTiO}_3$ <sup>40,41</sup> and at polar/polar interfaces such as  $\text{LaAlO}_3/\text{KNbO}_3$ ,  $\text{LaAlO}_3/\text{KTaO}_3$ ,  $\text{LaAlO}_3/\text{NaNbO}_3$ , and  $\text{LaAlO}_3/\text{NaTaO}_3$ .<sup>42,43</sup> An important advantage of polar/polar interfaces is that the polar catastrophe occurs on both the film and the substrate sides; consequently, both layers can donate electrons to the interface, leading to a higher interfacial carrier density compared to polar/nonpolar and nonpolar/nonpolar interfaces. Zou *et al.*<sup>44</sup> successfully realized the polar/polar  $\text{LaTiO}_3/\text{KTaO}_3$  heterostructure, where  $\text{LaTiO}_3$  is a Mott insulator and  $\text{KTaO}_3$  is a band insulator. They reported a higher interfacial carrier density and carrier mobility than those observed in the polar/nonpolar LAO/STO interface.

The 2DEGs formed at oxide perovskite interfaces have attracted considerable attention because of their diverse potential applications. For example, the 2DEG at the LAO/STO interface has been explored for sensors,<sup>45</sup> field-effect transistors,<sup>14,30</sup> thermoelectric devices,<sup>46,47</sup> solar cells,<sup>48,49</sup> and nanophotodetectors.<sup>50</sup> In addition, the photoconductivity of 2DEGs offers promising opportunities for applications in optical switches, photodetectors, and holographic memory devices.<sup>28,29,50–53</sup>

Recently, heterointerfaces based on  $\text{KTaO}_3$  (KTO) have attracted increasing interest for several reasons. First, KTO possesses a cubic crystal structure over the entire temperature range and does not undergo structural phase transitions, which provides enhanced structural stability to heterostructures formed with KTO. Second, KTO hosts Ta  $5d$  electrons that are less localized than the Ti  $3d$  electrons in  $\text{SrTiO}_3$ , which can lead to higher mobility of the 2DEG formed in KTO-based heterostructures.<sup>22</sup> Third, KTO exhibits a strong spin-orbit coupling that is nearly an order of magnitude larger than that of STO, potentially giving rise to interesting Rashba-type physics and enabling applications in spintronic devices.<sup>22,54</sup>

Despite these advantages, only a limited number of KTO-based heterostructures capable of hosting a 2DEG at their interfaces have been explored, including  $\text{LaTiO}_3/\text{KTaO}_3$ ,  $\text{LaVO}_3/\text{KTaO}_3$ , and  $\text{EuO}/\text{KTaO}_3$ .<sup>22,44,54,55</sup> Wadehra *et al.* have grown thin films of  $\text{LaVO}_3$  (LVO) epitaxially on  $\text{TaO}_2$ -terminated KTO(001) substrates using pulsed laser deposition.<sup>22</sup> The temperature dependence of resistivity confirmed the existence of a 2DEG at the LVO/KTO interface when

the thickness of the LVO film exceeds 3 monolayers, although both bulk LVO and bulk KTO are insulating. The LVO/KTO interface exhibits a high-density and high-mobility 2DEG with a measured carrier density of  $\sim 10^{14}$  electrons/ $\text{cm}^2$  and a carrier mobility of  $\sim 600$   $\text{cm}^2 \text{V}^{-1} \text{s}^{-1}$  at 1.8 K.<sup>56</sup> Notably, this interfacial carrier density is approximately one order of magnitude larger than that of the polar/nonpolar LAO/STO interface.

Motivated by these experimental observations, we investigate the polar/polar LVO/KTO perovskite oxide interface, where LVO is a Mott insulator and KTO is a band insulator. The interface consists of LaO termination from the LVO side and  $\text{TaO}_2$  termination from the KTO side, consistent with the experimentally realized structure. Despite the experimental observation of a 2DEG at the LVO/KTO interface, theoretical investigations aimed at understanding its microscopic origin and characteristics remain limited. In this work, we employ first-principles density functional theory calculations to investigate the origin of the 2DEG at the LVO/KTO interface, examine its consistency with experimental observations, compare its properties with those of other oxide interfaces, and provide further insight into the characteristics of the interfacial 2DEG.

## II. COMPUTATIONAL DETAILS

Our calculations were performed within the framework of spin-polarized density functional theory (DFT), as implemented in the Quantum ESPRESSO (QE) package.<sup>57</sup> The Kohn–Sham equations were expanded in a plane-wave basis set with kinetic energy cutoffs of 40 Ry for the wavefunctions and 400 Ry for the charge densities. The interaction between ionic cores and valence electrons was described using ultrasoft pseudopotentials.<sup>58</sup> Exchange–correlation effects were treated within the generalized gradient approximation (GGA) using the Perdew–Burke–Ernzerhof (PBE) functional.<sup>59</sup> Since the systems under investigation exhibit strong electronic correlations, the DFT+ $U$  method was employed.<sup>60,61</sup> Structural optimizations were carried out using the Cococcioni and de Gironcoli approach,<sup>60</sup> which employs only the Hubbard  $U$  parameter, where  $U$  represents the on-site Coulomb repulsion, with “atomic” Hubbard projections. The electronic structure calculations were performed using the rotationally invariant scheme of Liechtenstein *et al.*<sup>61</sup>, which employs both the Hubbard  $U$  and  $J$  parameters, where  $J$  denotes the on-site exchange interaction, with “ortho-atomic” Hubbard projections. For the V  $3d$  orbitals, the values  $U = 5.65$  eV and  $J = 0.65$  eV were used, while for the Ta  $5d$  orbitals we employed  $U = 5.00$  eV and  $J = 0.0$  eV. The values of  $U$  and  $J$  for V  $3d$  were chosen to reproduce the experimental band gap of bulk LVO ( $\sim 1.1$  eV).<sup>62</sup> The  $U$  and  $J$  parameters for Ta were adopted from previous studies reported in the literature.<sup>63</sup>

For calculations on the bulk phases of the constituent

materials of the heterostructure, we considered cubic KTO (see Fig. 1(a), which is the stable structure at all temperatures) and both orthorhombic (see Fig. 1(b), the room-temperature structure) and tetragonal (see Fig. 1(c), the structure adopted when LVO is grown on a KTO(001) substrate) phases of LVO. Calculations on orthorhombic LVO and cubic KTO were performed using bulk unit cells containing 20 and 5 atoms, respectively. Although the ground-state structure of LVO is orthorhombic, experiments have shown that when LVO is deposited on KTO(001), the overlayer adopts a tetragonal structure.<sup>22</sup> Calculations on the tetragonal phase of LVO were performed using a unit cell containing 10 atoms in order to accommodate the A-type antiferromagnetic (A-AFM) ordering of the V atoms. For these bulk calculations, Brillouin zone (BZ) integrations were performed using Monkhorst–Pack<sup>64</sup>  $k$ -point meshes of  $8 \times 8 \times 6$  for orthorhombic LVO,  $8 \times 8 \times 4$  for tetragonal LVO, and  $8 \times 8 \times 8$  for cubic KTO.

When viewed along the [001] direction, a perovskite material  $ABO_3$  consists of alternating AO and  $BO_2$  layers; thus, one formula unit corresponds to a unit cell (uc) composed of two layers. Accordingly, KTO consists of alternating KO and  $TaO_2$  layers, whereas LVO consists of alternating LaO and  $VO_2$  layers. For the heterostructure calculations, we considered a slab consisting of 4 uc of LVO (i.e., 8 LVO layers) deposited pseudomorphically on a substrate comprising 8.5 uc of KTO (i.e., 17 KTO layers), as shown in Fig. 1(d). This structure is denoted as vacuum/(LVO)<sub>4</sub>/(KTO)<sub>8.5</sub>. At the LVO/KTO interface, the KTO side is terminated by a  $TaO_2$  layer, while the LVO side is terminated by a LaO layer, consistent with the experimental growth conditions.<sup>22</sup> The top and bottom surfaces of the slab correspond to  $VO_2$  and  $TaO_2$  layers, respectively. For the heterostructure calculations, the Brillouin zone was sampled using an  $8 \times 8 \times 1$   $k$ -point mesh. Marzari–Vanderbilt smearing<sup>65</sup> with a smearing width of 0.005 Ry was employed to treat the discontinuity in the occupation function. All atomic coordinates were relaxed using the Broyden–Fletcher–Goldfarb–Shanno (BFGS) algorithm until the forces acting on each atom were less than 0.001 Ry/Bohr. For the slab structures, the in-plane lattice constants were fixed to the optimized lattice constant of bulk KTO. For the electronic structure calculations, the  $z$ -coordinates of the atoms were kept fixed.

### III. RESULTS AND DISCUSSION

#### A. Geometry and electronic structure of the constituents: cubic KTO, orthorhombic LVO and tetragonal LVO

We first determined the DFT optimized lattice parameters and atomic coordinates of bulk LVO and bulk KTO. The calculated structural parameters are summarized in Table I. Our PBE-GGA lattice parameters are

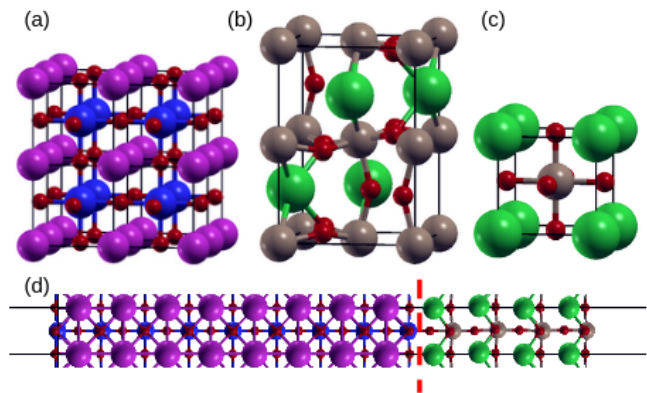


FIG. 1. Atomic structures of (a) cubic  $KTaO_3$ , (b) orthorhombic  $LaVO_3$ , (c) tetragonal  $LaVO_3$ , and (d) the vacuum/(LVO)<sub>4</sub>/(KTO)<sub>8.5</sub> slab. The dashed red line indicates the interface. Color code: purple (K), blue (Ta), red (O), green (La), and brown (V).

System	Lattice Parameter	Calc. (Ours)	Calc. (Previous)	Expt.
Orthorhombic LVO	$a$	5.547	5.632 <sup>66</sup>	5.555 <sup>67</sup>
	$b$	5.571	5.614 <sup>66</sup>	5.553 <sup>67</sup>
	$c$	7.952	7.843 <sup>66</sup>	7.848 <sup>67</sup>
Tetragonal LVO	$a$	4.011	–	–
	$c$	3.953	–	–
Cubic KTO	$a$	4.011	4.031 <sup>68</sup>	3.989 <sup>69</sup>

TABLE I. The lattice parameters of the bulk systems obtained from our DFT calculations, compared with values reported in previous theoretical studies and experiments. All values are in Å. We note that tetragonal LVO is a hypothetical structure that is not known to exist in the bulk phase.

in good agreement with previous DFT studies as well as with available experimental values. The optimized crystal structures are shown in Fig. 1. Bulk KTO adopts a cubic crystal structure (see Fig. 1(a)) and remains non-magnetic over the entire temperature range.<sup>70</sup> Bulk LVO exhibits a monoclinic structure below 140 K with C-type antiferromagnetic (C-AFM) ordering, whereas above 140 K it becomes non-magnetic (NM) and crystallizes in an orthorhombic structure.<sup>71</sup> In the present work, we considered the room-temperature orthorhombic phase of LVO, shown in Fig. 1(b).

In addition, we examined a hypothetical tetragonal structure of bulk LVO (see Fig. 1(c)). This structure was considered because experiments have shown that LVO layers grown on a KTO(001) substrate adopt a tetragonal symmetry, with the in-plane lattice parameters constrained by the substrate. Accordingly, the in-plane lattice constants were fixed to the optimized lattice constant of bulk KTO ( $a_{KTO} = 4.011$  Å), while the out-of-plane lattice constant obtained from our DFT optimization is 3.952 Å. Our calculations further indicate that tetragonal

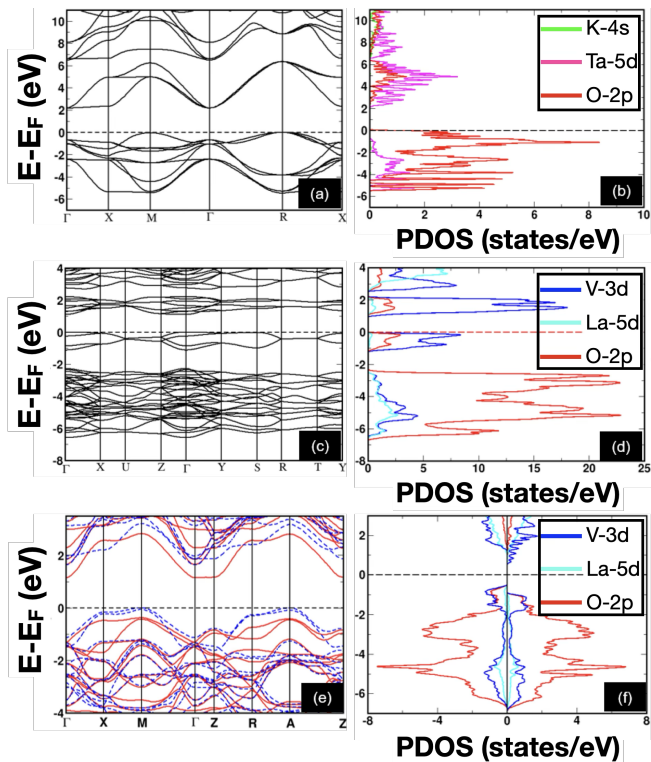


FIG. 2. Electronic band structures and orbital-projected density of states (PDOS) of (a)–(b) cubic  $\text{KTaO}_3$ , (c)–(d) orthorhombic  $\text{LaVO}_3$ , and (e)–(f) tetragonal  $\text{LaVO}_3$ . In (e), solid red and dashed blue lines indicate the spin-up and spin-down bands, respectively. Color code of PDOS: magenta (Ta 5d), red (O 2p), blue (V 3d), cyan (La 5d), and green (K 4s) orbitals. The horizontal dashed black line represents the Fermi level of the corresponding system.

LVO stabilizes in an A-type antiferromagnetic (A-AFM) configuration<sup>72</sup> of the V atoms, which corresponds to antiferromagnetic stacking of ferromagnetically aligned layers. Fig. 1(d) shows the slab structure of the LVO/KTO interface, namely the vacuum/(LVO)<sub>4</sub>/(KTO)<sub>8.5</sub> slab.

In Fig. 2, we present the calculated electronic band structures along with the corresponding orbital-projected densities of states (PDOS) for cubic KTO, orthorhombic LVO, and tetragonal LVO. Since cubic KTO and orthorhombic LVO are non-magnetic, their band structures are represented by solid black lines (see Fig. 2(a) and (c)). In contrast, tetragonal LVO exhibits A-type antiferromagnetic (A-AFM) ordering of the V atoms; therefore, the spin-polarized band structure is shown for this phase (see Fig. 2(e)), where solid red and dashed blue lines represent spin-up and spin-down bands, respectively.

A clear band gap is observed at the Fermi level (indicated by the horizontal dashed black or red line) between the valence band maximum (VBM) and the conduction band minimum (CBM), indicating that all three bulk phases are insulating and do not possess mobile charge carriers. For cubic KTO, Fig. 2(a) shows that the VBM lies at the R point in the Brillouin zone (BZ),

while the CBM is located at the  $\Gamma$  point. We note that the energies at the M and R points are nearly degenerate. Consequently, bulk KTO exhibits an indirect band gap of 2.18 eV, which is smaller than the experimentally measured value of 3.6 eV.<sup>73</sup> This underestimation arises from the use of the PBE-GGA exchange–correlation functional in our DFT calculations. Nevertheless, the calculated band gap is consistent with previous theoretical studies.<sup>68</sup> Since KTO is a band insulator, the DFT+ $U$  method does not significantly correct this band-gap underestimation. The PDOS of cubic KTO (see Fig. 2(b)) shows that the valence bands are predominantly derived from O 2p orbitals, with a small hybridization with Ta 5d states, indicating covalent bonding between O and Ta atoms. The conduction bands are mainly composed of Ta 5d states, with minor contributions from O 2p orbitals.

For orthorhombic LVO, our calculations yield a band gap of 1.1 eV, which is in excellent agreement with the experimentally reported value.<sup>62</sup> We verified that when  $U = J = 0$  eV or smaller values are used, the system becomes metallic or exhibits only a small band gap, which is inconsistent with experimental observations. Thus, an appropriate choice of  $U$  and  $J$ , corresponding to a proper treatment of electron correlations, is necessary to reproduce the experimental band gap of orthorhombic LVO. This behavior confirms that LVO is a Mott insulator. As shown in Fig. 2(c), orthorhombic LVO exhibits a direct band gap at the  $\Gamma$  point. The band structure shows a completely filled lower Hubbard band in the energy range  $[-1.1, 0]$  eV and an empty upper Hubbard band in the range  $[1.1, 2.2]$  eV. The PDOS (see Fig. 2(d)) indicates that both the VBM (lower Hubbard band) and the CBM (upper Hubbard band) are primarily contributed by V 3d orbitals, with a small hybridization with O 2p orbitals.

For tetragonal LVO, the spin-up and spin-down bands are shown by solid red and dashed blue lines, respectively (see Fig. 2(e)). Our calculations indicate that tetragonal LVO is also insulating, with an indirect band gap of 1.15 eV. The magnetic moments on the two V atoms in the unit cell are found to be  $1.50 \mu_B$ . The valence bands are mainly derived from O 2p orbitals, with minor contributions from V 3d and La 5d states. In contrast, the conduction bands are dominated by V 3d states, with small hybridization from O 2p and La 5d orbitals.

## B. Magnetic ground state of the LVO/KTO heterostructure

Previous DFT calculations on the LVO/KTO heterostructure did not include spin polarization.<sup>74</sup> In the present work, spin polarization was explicitly considered due to the presence of magnetic 3d V and 5d Ta atoms. To determine the magnetic ground state of the heterostructure, we examined the preferred magnetic ordering of the V atoms, which are expected to carry larger magnetic moments compared to the Ta atoms. Specifically, we considered non-magnetic (NM), ferromagnetic (FM), A-

type antiferromagnetic (A-AFM), C-type antiferromagnetic (C-AFM), and G-type antiferromagnetic (G-AFM) configurations of the V atoms.

Magnetic ordering of V atoms	$\Delta E$ (meV/f.u.)
NM	6433
FM	21
A-AFM	0
C-AFM	352
G-AFM	459

TABLE II. Comparison of the total energies of different magnetic orderings of V atoms in the vacuum/(LVO)<sub>4</sub>/(KTO)<sub>8.5</sub> slab.  $\Delta E$  denotes the total energy difference of a given magnetic ordering with respect to the lowest-energy configuration (A-AFM).  $\Delta E$  is calculated per formula unit of the LVO/KTO heterostructure.

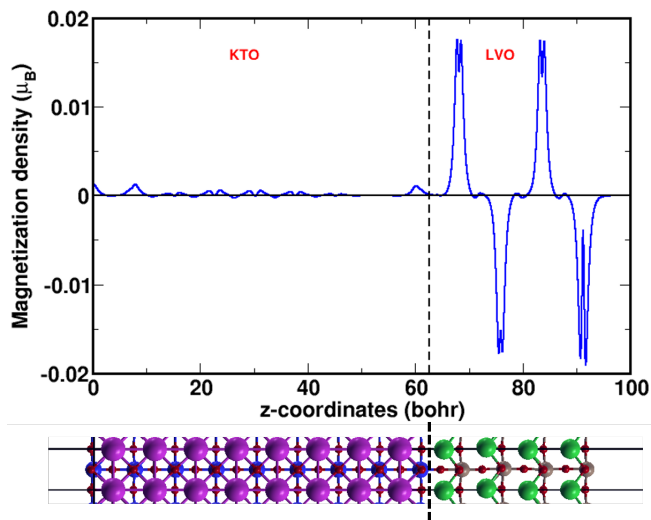


FIG. 3. Planar-averaged magnetization density as a function of the  $z$  coordinate for the vacuum/(LVO)<sub>4</sub>/(KTO)<sub>8.5</sub> slab. The atomic structure of the slab is shown below to identify the layers at each  $z$  position. The vertical dashed black line indicates the interface. Color code: purple (K), blue (Ta), red (O), green (La), and brown (V).

The total energies for these magnetic configurations were compared on a per formula unit basis, and the results are summarized in Table II. Among the configurations considered, the A-AFM ordering is found to be the most energetically favorable, while the NM configuration has the highest energy. This result highlights the limitation of the previous DFT study,<sup>74</sup> which assumed an NM configuration. Therefore, all subsequent calculations for the LVO/KTO heterostructure were performed using the A-AFM ordering of the V atoms. Recall that the V atoms favor A-AFM ordering in tetragonal LVO; consequently, the heterostructure also retains this A-AFM configuration when the KTO substrate is introduced.

To further analyze the magnetic properties of the system, we calculated the planar-averaged magnetization (or spin-polarization) density along the direction perpendicular to the interface. The planar average was taken over the  $xy$ -plane, which is parallel to the interface, and is defined as

$$\tilde{m}(z) = \frac{1}{A} \int m(x, y, z) dx dy, \quad (1)$$

where  $m(x, y, z) = m(\mathbf{r}) = n_{\uparrow}(\mathbf{r}) - n_{\downarrow}(\mathbf{r})$ , with  $n_{\uparrow}(\mathbf{r})$  and  $n_{\downarrow}(\mathbf{r})$  representing the spin-up and spin-down electron densities, respectively, at position  $\mathbf{r}$  in space, and  $A$  denotes the surface area of the  $xy$ -plane.

The variation of  $\tilde{m}(z)$  as a function of  $z$  is shown in Fig. 3. A positive value of  $\tilde{m}(z)$  corresponds to  $m(\mathbf{r}) > 0$ , indicating that the spin-up electron density exceeds the spin-down electron density at position  $\mathbf{r}$ . Conversely,  $\tilde{m}(z) < 0$  implies that the spin-down electron density is larger than the spin-up electron density. As evident from Fig. 3, the magnetization density is significant within the VO<sub>2</sub> layers and alternates between positive and negative values along the  $z$  direction. This behavior arises from the presence of magnetic V 3d atoms, which possess substantial magnetic moments and exhibit alternating spin-up and spin-down orientations due to the A-AFM ordering. In contrast, the atoms in the other layers carry negligible magnetic moments, corresponding to  $\tilde{m}(z) \approx 0$ . The Ta atoms at the interface and at the surface exhibit small induced magnetic moments, which appear as weak peaks in the magnetization density near the interfacial and surface TaO<sub>2</sub> layers. Although bulk KTO is non-magnetic, a small magnetic moment is induced on the interfacial TaO<sub>2</sub> layer due to the proximity of the magnetic LVO layer.

### C. Polar distortions in the LVO/KTO heterostructure

We note that the optimized slab of the LVO/KTO heterostructure, namely vacuum/(LVO)<sub>4</sub>/(KTO)<sub>8.5</sub>, shown in Fig. 1(d), has LaO and TaO<sub>2</sub> layers at the interface, while the two surfaces facing the vacuum are terminated by VO<sub>2</sub> layer on the LVO side and TaO<sub>2</sub> layer on the KTO side. Since the in-plane lattice parameters are fixed at the optimized lattice constant of bulk KTO ( $a_{\text{KTO}} = 4.011$  Å), the LVO film experiences tensile strain when grown on the KTO(001) substrate. However, the magnitude of this strain is small ( $< 1\%$ ), which allows the LVO film to be grown epitaxially and pseudomorphically on the KTO substrate.

To analyze the structural distortions in the LVO/KTO heterostructure, we calculate the “relative displacement” or “polar distortion” defined as  $(z_{\text{cation}} - z_{\text{anion}})$ , where  $z_{\text{cation}}$  and  $z_{\text{anion}}$  denote the average  $z$ -coordinates of the cations and anions, respectively, in each layer of the relaxed slab structure. The layer-resolved polar distortion

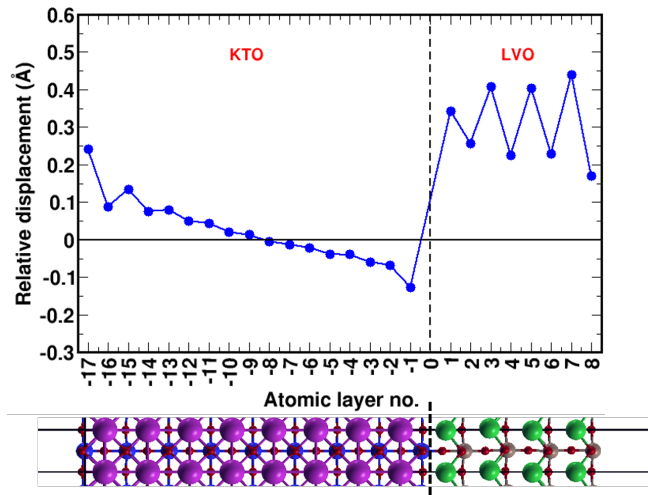


FIG. 4. Relative cation-anion displacement for each layer in the vacuum/(LVO)<sub>4</sub>/(KTO)<sub>8.5</sub> slab. Atomic layers are numbered by positive and negative integers for the LVO and KTO regions, respectively, starting from the interface. The atomic structure of the slab is shown below to identify the layers. The vertical dashed black line indicates the interface. Color code: purple (K), blue (Ta), red (O), green (La), and brown (V).

is shown in Fig. 4. The layers are indexed by positive and negative integers for the LVO and KTO regions, respectively, starting from the interface. The corresponding atomic structure is also shown below each layer index for clarity.

On the LVO side, the polar distortion is positive and relatively large for both the LaO and VO<sub>2</sub> layers. This indicates that  $z_{\text{cation}}$  is larger than  $z_{\text{anion}}$ , implying that within each layer the O<sup>2-</sup> anions are displaced towards the interface, while the La<sup>3+</sup> or V<sup>3+</sup> cations move away from the interface. Consequently, a small electric dipole moment is generated in each layer, pointing from the interface towards the surface on the LVO side. The cumulative effect of these layer-resolved dipoles produces a significant polarization, similar to that observed in ferroelectric materials, directed away from the interface towards the surface. This is the reason why the relative cation-anion displacement is often referred to as “polar distortion”. We further observe that the magnitude of the polar distortion is larger in the LaO layers than in the VO<sub>2</sub> layers. Moreover, as one moves away from the interface, the polar distortion increases in the LaO layers while it decreases in the VO<sub>2</sub> layers.

On the KTO side, the ferroelectric-like polar distortion is comparatively smaller in magnitude than that on the LVO side. It is negative near the interface and becomes positive near the surface, with a vanishing value in the middle region of the slab. Near the interface,  $z_{\text{cation}}$  is smaller than  $z_{\text{anion}}$ , indicating that the O<sup>2-</sup> anions are displaced towards the interface, while the K<sup>+</sup> or Ta<sup>5+</sup> cations move away from the interface, resulting in a polarization pointing away from the interface. Thus, near

the interface, the polarization vectors on the LVO and KTO sides are oriented in opposite directions. Because the KTO substrate is relatively thick, this polar distortion decays rapidly away from the interface and becomes negligible in the central region of the KTO slab.

Near the surface of KTO,  $z_{\text{cation}}$  becomes larger than  $z_{\text{anion}}$ , indicating that the O<sup>2-</sup> anions are displaced towards the surface, while the K<sup>+</sup> or Ta<sup>5+</sup> cations move away from the surface. This produces a polarization pointing from the surface towards the interface. Consequently, two polarization regions are formed within the KTO layer, with polarization vectors oriented in opposite directions. Similar structural behavior has been reported in other perovskite oxide heterostructures such as LaTiO<sub>3</sub>/SrTiO<sub>3</sub>, LaAlO<sub>3</sub>/SrTiO<sub>3</sub>, and LaScO<sub>3</sub>/BaSnO<sub>3</sub>.<sup>75–77</sup>

#### D. Electronic band structure: Emergence of metallicity

Having established the structural properties, we next examine the electronic structure of the LVO/KTO heterostructure. The spin-polarized electronic band structure of the vacuum/(LVO)<sub>4</sub>/(KTO)<sub>8.5</sub> slab with A-AFM ordering of the V atoms is shown in Fig. 5. The BZ of this slab structure is square; therefore, the band structure is plotted along the high-symmetry path M–Γ–X–M. The spin-up and spin-down bands are represented by solid red and dashed blue lines, respectively. Partially occupied bands are observed to cross the Fermi level, indicating that the LVO/KTO heterostructure exhibits metallic behaviour. This result is particularly notable because the constituent bulk materials, LVO and KTO, are both insulating. Thus, when these two insulators – a Mott insulator (LVO) and a band insulator (KTO) – are combined to form the heterostructure, metallicity emerges at the interface.

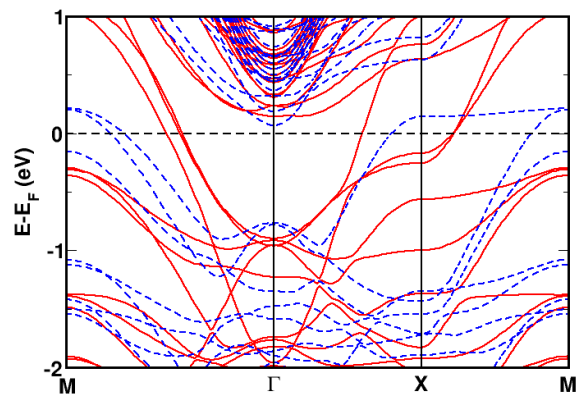


FIG. 5. Band structure of the vacuum/(LVO)<sub>4</sub>/(KTO)<sub>8.5</sub> slab. Solid red and dashed blue lines represent the spin-up and spin-down bands, respectively. The horizontal dashed black line indicates the Fermi level of the system.

A prominent feature of the band structure is the pres-

ence of a spin-up band with a parabolic dispersion ( $E \sim k^2$ ) around the  $\Gamma$  point. This band touches an energy of approximately  $-2$  eV and crosses the Fermi level, thereby contributing to the metallic character of the system. The parabolic dispersion is characteristic of a free-electron-like band. In addition, a group of conduction bands is observed around the  $\Gamma$  point just above the Fermi level for both spin channels, which also display parabolic dispersions. These bands are expected to contribute to the 2DEG formed at the interface. While the band structure clearly indicates the metallic nature of the LVO/KTO heterostructure as a whole and the presence of free carriers in it, it does not directly reveal the specific atomic layers that host these electrons.

### E. Origin of the 2DEG: Layer-resolved PDOS reveals “electronic reconstruction”

The electronic band structure provides direct evidence that the LVO/KTO heterostructure is conducting; however, it does not reveal which atomic layers primarily host the mobile electrons, nor does it provide insight into the fundamental origin of the metallicity in this heterostructure. These two important aspects are examined in the present and the following subsections. To gain further insight into the origin of the metallic behavior, we compute the layer-resolved PDOS of the vacuum/(LVO)<sub>4</sub>/(KTO)<sub>8.5</sub> slab. The results are shown in Fig. 6, where the atomic layers are indexed by positive and negative integers for the LVO and KTO parts, respectively, starting from the interface. For each layer, the PDOS of the spin-up and spin-down states are plotted along the positive and negative  $y$ -axes, respectively. Only those states that cross the Fermi level are partially occupied and therefore contribute to electrical conduction.

We observe that, except for the interfacial TaO<sub>2</sub>, surface TaO<sub>2</sub>, and surface VO<sub>2</sub> layers, all other layers remain insulating. The layer-resolved PDOS clearly demonstrates that the conducting states originate at the interface and that the mobile electrons are strongly confined to this region, while the neighboring layers remain insulating. This observation is consistent with experimental results, which indicate that the 2DEG is highly localized near the interface. Such strong spatial confinement highlights the two-dimensional character of the electron gas: the conduction electrons can move freely within the  $xy$ -plane, while they remain confined within a narrow region perpendicular to the interface.

At the interface (layer  $-1$ ), the bottom of the conduction band formed by Ta  $5d$  spin-up states crosses the Fermi level. This indicates that the 2DEG is primarily hosted by the interfacial Ta  $5d$  spin-up states, further confirming that the electron gas formed at the LVO/KTO interface is spin-polarized, with only spin-up electrons contributing to conduction. The adjacent TaO<sub>2</sub> layer (layer  $-3$ ) and the VO<sub>2</sub> layer closest to the interface

(layer 2) contribute only weakly to the 2DEG. The occupied states responsible for the 2DEG extend from the CBM up to the Fermi level. Our calculations further indicate that the 2DEG predominantly resides on the KTO side rather than on the LVO side, which is consistent with experimental observations.<sup>55</sup> The inner or bulk-like layers of both the LVO and KTO regions remain insulating and therefore do not contribute to the 2DEG.

The Fermi level also intersects the electronic states of the surface TaO<sub>2</sub> layer (layer  $-17$ ) and the surface VO<sub>2</sub> layer (layer 8), although these layers are located away from the interface. For the surface TaO<sub>2</sub> layer, the Fermi level crosses the spin-up Ta  $5d$  conduction bands, indicating the presence of mobile electrons between the CBM and the Fermi level at this layer. In contrast, for the surface VO<sub>2</sub> layer, the Fermi level intersects the V  $3d$  and O  $2p$  valence bands (spin-down states), indicating the presence of mobile holes extending from the Fermi level up to the VBM. Thus, at the surface layers, the mobile electrons are spin-up while the mobile holes are spin-down.

On the LVO side, moving away from the interface, the valence states gradually approach the Fermi level and eventually cross it at the surface VO<sub>2</sub> layer, thereby creating holes. These holes arise due to the depletion of electrons in this layer that are transferred to the interfacial TaO<sub>2</sub> layer. The transferred electrons occupy the Ta  $5d$  conduction-band states and form the 2DEG at the interface. In particular, electrons migrate from the V  $3d$  and O  $2p$  surface valence bands of the LVO film to the Ta  $5d$  conduction bands at the interface. This charge transfer is driven by the presence of an internal electric field on the LVO side (opposite to the direction of polarization discussed in Sec. C). This mechanism, in which electrons are transferred from the surface of the polar LVO film to the LVO/KTO interface, is commonly referred to as “electronic reconstruction”. Our calculations clearly identify this electronic reconstruction mechanism as the fundamental origin of the 2DEG at this interface.

A previous DFT study<sup>74</sup> did not consider spin polarization and therefore could not establish the electronic reconstruction mechanism convincingly. Their charge-density difference plots showed larger electron accumulation on the LVO side, which is inconsistent with experimental observations indicating that the 2DEG primarily resides on the KTO side. Moreover, the calculated amount of electron transfer was two orders of magnitude smaller than the experimentally observed value of  $\sim 10^{14}$  electrons/cm<sup>2</sup>. Another previous theoretical study<sup>78</sup> included spin polarization and suggested electronic reconstruction as the mechanism responsible for the formation of the 2DEG at the LVO/KTO interface. However, that work did not provide clear evidence for this mechanism from layer-resolved PDOS analysis, and their charge-density difference plots did not reveal electron depletion or hole formation at the surface of the LVO film.

In summary, our calculations demonstrate that the 2DEG originates from the interfacial Ta  $5d$  spin-up

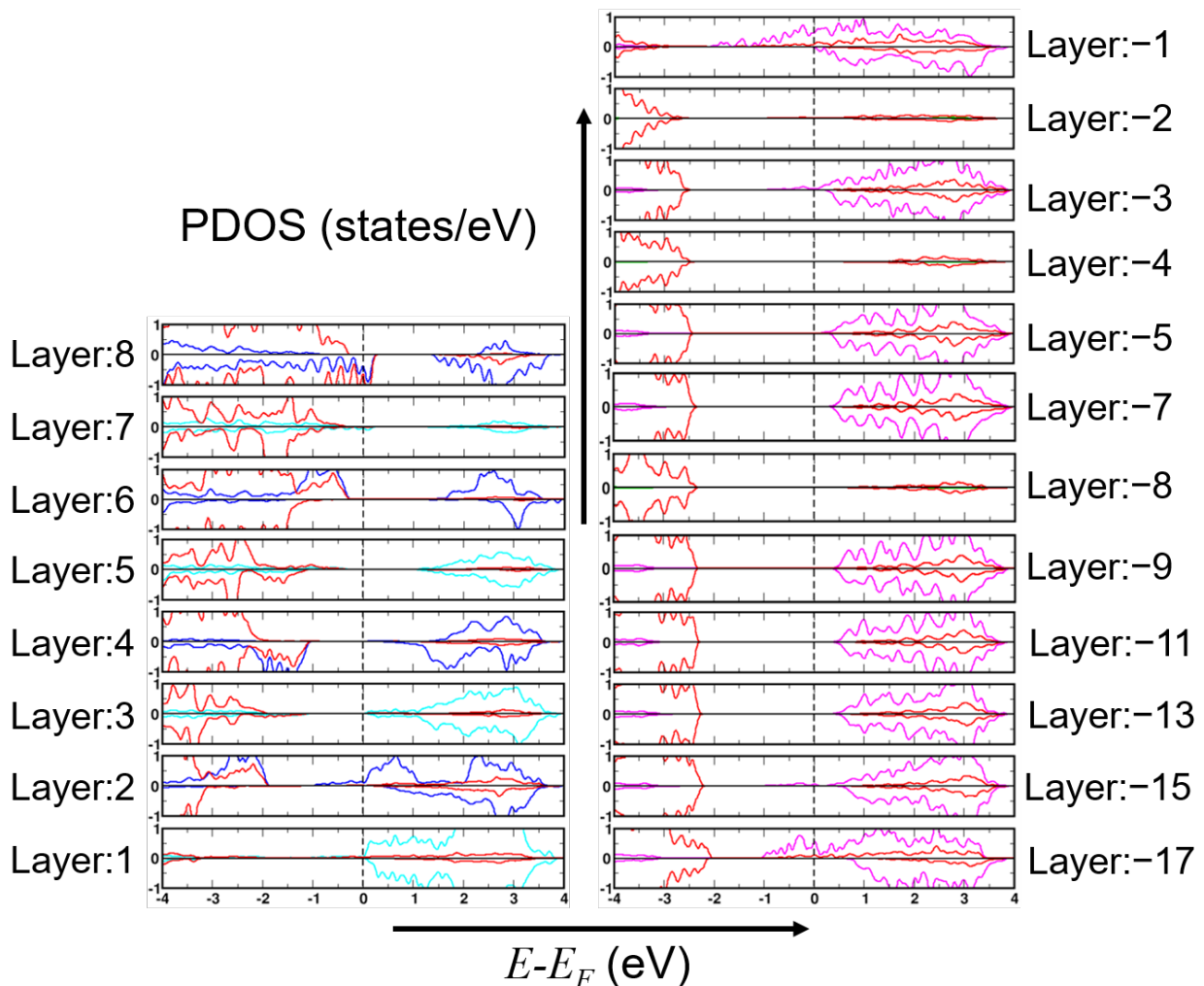


FIG. 6. Layer-resolved orbital-projected density of states (PDOS) of the vacuum/ $(\text{LVO})_4/(\text{KTO})_{8.5}$  slab. Atomic layers are numbered by positive and negative integers for the LVO region (left) and the KTO region (right), respectively, starting from the interface. The vertical dashed black line indicates the Fermi level. Some even-numbered layers (KO layers) away from the interface on the KTO side are not shown, as they do not contribute to the 2DEG. PDOS of spin-up and spin-down states are shown on the positive and negative  $y$  axis, respectively. Color code of PDOS: magenta (Ta  $5d$ ), red (O  $2p$ ), blue (V  $3d$ ), cyan (La  $5d$ ), and green (K  $4s$ ).

states, occupying the energy range from the CBM up to the Fermi level. The electron gas is sharply confined to the interface, exhibits spin polarization, and arises from the electronic reconstruction mechanism at the LVO/KTO interface.

#### F. Ultralow effective mass and high mobility of the 2DEG

We next analyze the band structure (see Fig. 5) in greater detail in order to identify the specific bands that host the 2DEG at the interface and the bands that donate electrons from the surface  $\text{VO}_2$  layer, as these states play a crucial role in the formation of the 2DEG. Guided by the layer-resolved PDOS (see Fig. 6), we therefore project

the band structure of the vacuum/ $(\text{LVO})_4/(\text{KTO})_{8.5}$  slab onto the Ta  $5d$  orbitals of the interfacial  $\text{TaO}_2$  layer and onto the V  $3d$  and O  $2p$  orbitals of the surface  $\text{VO}_2$  layer.

We find that, for the interfacial  $\text{TaO}_2$  layer, only the spin-up Ta  $5d_{xy}$  orbital crosses the Fermi level. In contrast, for the surface  $\text{VO}_2$  layer, all five  $d$  orbitals of the V atoms (spin-down channel only) and all three  $p$  orbitals of the O atoms (spin-down channel only) cross the Fermi level. These results are shown in Fig. 7, where the color scale represents the magnitude of the orbital contribution to each band: blue–green indicates a lower contribution, whereas orange–red indicates a higher contribution.

Interestingly, the Ta  $5d_{xy}$  orbitals produce a parabolic band around the  $\Gamma$  point (touching it at  $\sim -2$  eV) that crosses the Fermi level and therefore contributes to electron conduction (see Fig. 7(a)). The curvature

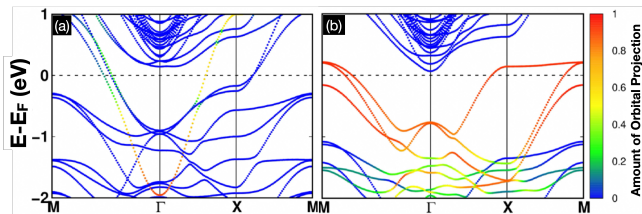


FIG. 7. Band structure of the vacuum/(LVO)<sub>4</sub>/(KTO)<sub>8.5</sub> slab projected onto the (a) Ta 5d<sub>xy</sub> orbitals (spin-up states) of the interfacial TaO<sub>2</sub> layer and (b) V 3d (spin-down states) and O 2p orbitals (spin-down states) of the surface VO<sub>2</sub> layer. The horizontal dashed black line indicates the Fermi level. The color scale represents the magnitude of the orbital contribution.

of this parabolic band confirms its electron-like character. The 2DEG at the LVO/KTO interface is hosted by this band, which further confirms the free-electron-like behavior of the interfacial carriers, as its dispersion follows the  $E \propto k^2$  relation. Moreover, the  $d_{xy}$  character of this band indicates that the mobile electrons forming the 2DEG can move freely within the  $xy$ -plane while remaining strongly confined along the  $z$ -direction. This behavior highlights the strongly two-dimensional character of the electron gas, which is localized near the interface on the KTO side. The other parabolic bands appearing just above the Fermi level around the  $\Gamma$  point mainly originate from the Ta 5d orbitals of the other TaO<sub>2</sub> layers.

Figure 7(b) shows that the spin-down states of the V 3d and O 2p orbitals of the surface VO<sub>2</sub> layer contribute to several bands that cross the Fermi level. The curvature of these bands confirms their hole-like character, indicating that they belong to the valence band. Thus, in addition to the layer-resolved PDOS, the band curvature clearly reveals the presence of electrons at the interfacial TaO<sub>2</sub> layer and holes at the surface VO<sub>2</sub> layer. The spin-up electron-like bands and spin-down hole-like bands are also fully consistent with the layer-resolved PDOS results (see layers  $-1$  and  $8$  in Fig. 6).

To estimate the effective mass of the 2DEG electrons, given by  $m^* = \hbar^2 / \frac{d^2 E}{dk^2}$ , we fit the red band in Fig. 7(a), originating from the Ta 5d<sub>xy</sub> spin-up states, with a parabolic function near the  $\Gamma$  point. Our calculation yields an effective mass of  $m^* = 0.11 m_0$ , where  $m_0$  is the free electron mass. To the best of our knowledge, this value is significantly smaller than those reported for other oxide heterostructures. For example, in the extensively studied LaAlO<sub>3</sub>/SrTiO<sub>3</sub> system, the reported effective mass lies in the range  $m^* = 0.4\text{--}0.6 m_0$ .<sup>79,80</sup> Within the Drude model, the electron mobility is given by  $\mu = \frac{e\tau}{m^*}$ , where  $e$  is the electronic charge and  $\tau$  is the average time between two successive scattering events of an electron with ions. The smaller effective mass of the interfacial electrons therefore leads to higher carrier mobility at the LVO/KTO interface compared to the widely studied LAO/STO system. This enhanced mobility arises because the 2DEG in the LVO/KTO heterostructure is

hosted by Ta 5d orbitals, which are more spatially extended and delocalized than the Ti 3d orbitals responsible for the 2DEG at the LAO/STO interface.

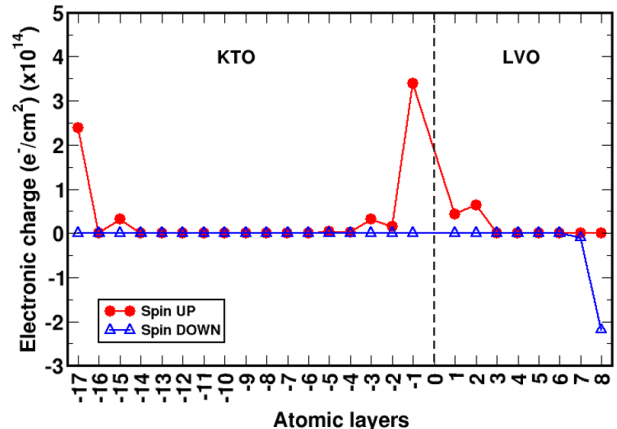


FIG. 8. Carrier density (per unit interfacial area) for each layer of the vacuum/(LVO)<sub>4</sub>/(KTO)<sub>8.5</sub> slab. Atomic layers are numbered by positive and negative integers for the LVO and KTO regions, respectively, starting from the interface. The vertical dashed black line (at 0) indicates the interface. Filled red circles and open blue triangles correspond to spin-up and spin-down states, respectively. Positive and negative  $y$  values correspond to electrons and holes, respectively.

### G. Layer-resolved carrier density

Next, we calculate the carrier density for each layer of the vacuum/(LVO)<sub>4</sub>/(KTO)<sub>8.5</sub> slab by integrating the density of states of each layer either from the CBM up to the Fermi level to obtain the electron density or from the Fermi level up to the VBM to obtain the hole density. The density of states of each layer is integrated for both the majority and minority spin channels. A similar procedure has been employed previously for other systems.<sup>81</sup> The resulting layer-resolved and spin-resolved electronic charge is shown in Fig. 8, where filled red circles and open blue triangles represent spin-up and spin-down states, respectively. The charges arising from electrons and holes are plotted along the positive and negative  $y$ -axes, respectively. States that do not cross the Fermi level do not contribute any free charge carriers.

We observe that the interfacial TaO<sub>2</sub> layer (layer  $-1$ ) possesses the largest electronic charge, with a spin-up electron density of  $3.39 \times 10^{14}$  electrons/cm<sup>2</sup>. This layer therefore serves as the primary source of the mobile electrons forming the 2DEG at the LVO/KTO interface. This value agrees well with the experimentally measured density of  $\sim 1.02 \times 10^{14}$  electrons/cm<sup>2</sup>,<sup>55</sup> and is about one order of magnitude larger than that reported for the well-known LAO/STO interface, which typically exhibits an electron density of  $\sim 10^{13}$  electrons/cm<sup>2</sup>. The enhanced electron density at the LVO/KTO interface can be attributed to the fact that both the polar LVO film and

the polar KTO substrate contribute electrons to the interface, whereas in the LAO/STO system only the polar LAO film donates electrons.

Notably, the spin-down electron density at the interface is zero, indicating that the 2DEG is fully spin-polarized. All KO layers remain insulating and do not host any free charge carriers. The next TaO<sub>2</sub> layer (layer -3) and the two closest layers on the LVO side (layers 1 and 2) contain only a very small density of spin-up electrons. The electron density decays rapidly away from the interface on both the LVO and KTO sides, demonstrating that the 2DEG is strongly confined to the interface and therefore possesses a strictly two-dimensional character. No spin-down free electrons are present in the system, as indicated by the absence of open blue triangles along the positive  $y$ -axis. These results confirm that the 2DEG is primarily hosted by the interfacial TaO<sub>2</sub> layer on the KTO side, consistent with experimental observations.<sup>55</sup> In addition, the two surface TaO<sub>2</sub> layers of the KTO region (layers -17 and -15) also contain mobile spin-up electrons.

The surface VO<sub>2</sub> layer possesses approximately  $2.2 \times 10^{14}$  holes/cm<sup>2</sup> in the spin-down channel, as shown along the negative  $y$ -axis in Fig. 8. As discussed earlier, these holes are created because electrons are transferred from this layer to the interfacial TaO<sub>2</sub> layer in order to avoid the polar catastrophe at the LVO/KTO interface. Since both LVO and KTO are polar materials composed of alternating positively and negatively charged layers, electrons are transferred from the surfaces of both the LVO film and the KTO substrate to stabilize the electrostatic potential and prevent polar catastrophe on both sides of the heterostructure.

## H. Spatial distribution of the 2DEG charge density

To visualize the spatial distribution of the interfacial electrons, we next compute the band-decomposed charge density, given by  $|\psi_{n\mathbf{k}\sigma}(\mathbf{r})|^2$ . Here the band index  $n$  corresponds to the parabolic 2DEG band arising from the interfacial Ta  $5d_{xy}$  orbitals (see the red band in Fig. 7(a)). The wave vector  $\mathbf{k}$  is chosen at the  $\Gamma$  point, and the spin state is taken as  $\sigma = \uparrow$ , corresponding to the spin-up electrons that constitute the interfacial 2DEG.

The resulting band-decomposed charge density is shown in Fig. 9. The cyan lobes represent the isosurface of the electron density associated with the 2DEG at the LVO/KTO interface. We observe that these lobes are distributed predominantly parallel to the interface (in the  $xy$ -plane). This behavior arises because the 2DEG electrons originate mainly from the Ta  $5d_{xy}$  orbitals, whose spatial character lies in the  $xy$  plane. Consequently, the electron density is strongly suppressed in the direction perpendicular to the interface (along the  $z$ -direction). This spatial distribution indicates that the mobile electrons can move freely parallel to the interface through these lobes, while their motion remains strongly confined

along the  $z$ -direction. The band-decomposed charge density therefore provides direct real-space evidence for the strong confinement of the 2DEG around the LVO/KTO interface.

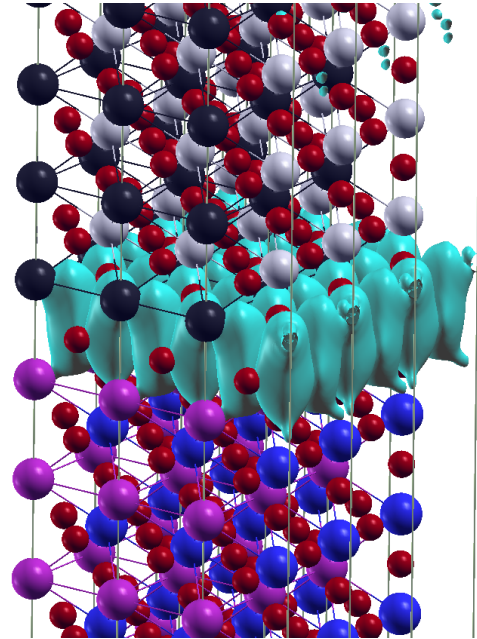


FIG. 9. Band-decomposed charge density  $|\psi_{n\mathbf{k}\uparrow}(\mathbf{r})|^2$  for the parabolic band of the interfacial TaO<sub>2</sub> layer at the  $\Gamma$  point corresponding to spin-up electrons that primarily contribute to the 2DEG at the interface. Cyan lobes represent the electron density forming the 2DEG. The lobes are connected within the plane parallel to the interface but are not extended in the perpendicular direction, indicating strong confinement of the 2DEG at the interface. Color code: purple (K), blue (Ta), red (O), black (La), and grey (V).

## I. Existence of a critical thickness

We next investigate whether a critical thickness of the LVO film is required for the LVO/KTO interface to become conducting, similar to the behavior observed in the LAO/STO heterointerface.<sup>82</sup> To examine this, we calculate the total density of states (TDOS) for heterostructure slabs with reduced thicknesses of both the film and the substrate. The TDOS of the vacuum/(LVO)<sub>3</sub>/(KTO)<sub>3</sub> and vacuum/(LVO)<sub>2</sub>/(KTO)<sub>6</sub> slabs are shown in Fig. 10, where spin-up and spin-down states are represented by red (positive  $y$ -axis) and blue (negative  $y$ -axis) lines, respectively.

For the vacuum/(LVO)<sub>3</sub>/(KTO)<sub>3</sub> slab, a clear gap is observed at the Fermi level, indicating that no states cross the Fermi level and the heterostructure remains insulating. This result suggests that when the thickness of the film and substrate is below a certain critical value, the LVO/KTO interface remains nonconducting. Our calculated result is consistent with experimental observa-

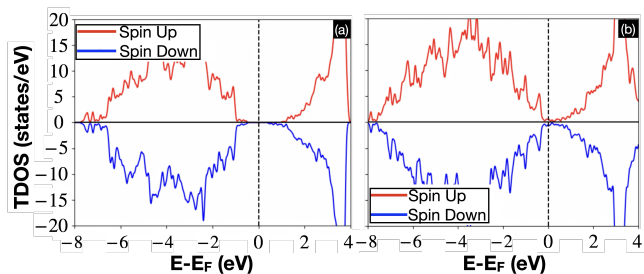


FIG. 10. Total density of states (TDOS) for heterostructures with reduced film and substrate thickness: (a) vacuum/(LVO)<sub>3</sub>/(KTO)<sub>3</sub> and (b) vacuum/(LVO)<sub>2</sub>/(KTO)<sub>6</sub> slabs. Red and blue lines correspond to spin-up and spin-down states, respectively.

tions, which show that the LVO/KTO interface remains insulating until three monolayers of LVO are grown on the KTO(001) substrate, beyond which the interface becomes metallic.<sup>22</sup> The existence of a critical thickness can be understood from electrostatic considerations. In polar/nonpolar or polar/polar heterostructures, the electrostatic potential increases with increasing film thickness. The system can tolerate this increasing potential only up to a certain thickness of the polar material; beyond this limit, electronic reconstruction occurs in order to avoid the polar catastrophe. Each heterostructure therefore has a threshold thickness beyond which the accumulated electrostatic potential becomes unsterable.

Unlike the LAO/STO system, in the LVO/KTO heterostructure both the film and the substrate are polar materials. As a result, the polar catastrophe can occur on both sides of the interface. Consequently, critical thicknesses may exist not only for the LVO film but also for the KTO substrate. Evidence for the occurrence of polar catastrophe on the KTO side can be obtained from the TDOS of the vacuum/(LVO)<sub>2</sub>/(KTO)<sub>6</sub> slab, where the LVO film thickness is reduced while the thickness of the KTO substrate is increased. In this case, states are observed to cross the Fermi level, indicating metallic behavior. This metallicity cannot originate from electronic reconstruction on the LVO side, since our earlier results (see Fig. 10(a)) show that the LVO/KTO heterostructure can tolerate the electrostatic potential up to 3 uc of LVO without undergoing reconstruction. Instead, the metallic behavior of the vacuum/(LVO)<sub>2</sub>/(KTO)<sub>6</sub> slab arises from the increased thickness of the KTO substrate, which can no longer sustain the growing electrostatic potential. As a result, electrons are transferred from the surface of the KTO substrate to the interface. This finding further supports our conclusion that, in the vacuum/(LVO)<sub>4</sub>/(KTO)<sub>8.5</sub> slab, electrons are transferred from the surfaces of both the LVO film and the KTO substrate to the interface.

#### IV. SUMMARY AND CONCLUSIONS

In summary, we employed first-principles density functional theory calculations to elucidate the microscopic origin of the two-dimensional electron gas (2DEG) at the interface between the band insulator KTaO<sub>3</sub> (KTO) and the Mott insulator LaVO<sub>3</sub> (LVO). Although both bulk constituents are insulating, the LVO/KTO heterostructure exhibits a robust metallic interface. Our results demonstrate that the simultaneous presence of polar layers in both LVO and KTO gives rise to polar discontinuities on either side of the interface, generating internal electric fields that point toward the interface from both the film and the substrate. This electrostatic instability drives an electronic reconstruction in which electrons migrate from the outer surfaces of the LVO film and the KTO substrate toward the interface, thereby preventing the polar catastrophe. As a consequence, holes accumulate in the surface VO<sub>2</sub> layer while electrons concentrate in the interfacial TaO<sub>2</sub> layer, forming a highly confined and spin-polarized 2DEG.

The interfacial electron gas is found to reside predominantly in Ta 5*d*<sub>xy</sub> orbitals, resulting in strong confinement perpendicular to the interface and carrier motion restricted to the interfacial plane. Notably, the spin-up parabolic band hosting the 2DEG exhibits an exceptionally small effective mass—substantially lower than that reported for the prototypical LaAlO<sub>3</sub>/SrTiO<sub>3</sub> interface—suggesting significantly enhanced carrier mobility. Furthermore, the calculated interfacial electron density is nearly an order of magnitude higher than that of the LaAlO<sub>3</sub>/SrTiO<sub>3</sub> system. Together, these findings establish the LVO/KTO heterointerface as a promising platform for realizing high-density, high-mobility 2DEGs in correlated oxide heterostructures, offering exciting opportunities for future oxide-based quantum and electronic devices.

#### ACKNOWLEDGEMENTS

A.D. gratefully acknowledges JNCASR, Bangalore, and the Department of Science and Technology (DST), Government of India, for financial support through his Ph.D. and postdoctoral fellowships. A.D. also acknowledges the computational facilities provided by the Sheikh Saqr Laboratory of ICMS, JNCASR, the TUE-CMS facility at JNCASR, and the PARAM Yukti supercomputer at JNCASR, Bangalore, under the National Supercomputing Mission (NSM). A.D. further acknowledges the supportive research environment at ASDU, Gudur. The author thanks Prof. Suvankar Chakraverty of INST, Mohali and Prof. Shobhana Narasimhan of JNCASR, Bangalore, for numerous fruitful discussions and intellectually stimulating ideas that significantly enriched this work.

## DATA AVAILABILITY

The data supporting the findings of this study are not publicly available due to technical constraints and resource limitations associated with preparing and hosting the dataset. However, the data are available from the authors upon reasonable request.

- 
- [1] Y. Tokura and H. Y. Hwang, Complex oxides on fire, *Nat. Mater.* **7**, 694 (2008).
- [2] J. Reiner, F. Walker, and C. Ahn, Atomically engineered oxide interfaces, *Science* **323**, 1018 (2009).
- [3] E. Dagotto, Complexity in strongly correlated electronic systems, *Science* **309**, 257 (2005).
- [4] H. Y. Hwang, Y. Iwasa, M. Kawasaki, B. Keimer, N. Nagaosa, and Y. Tokura, Emergent phenomena at oxide interfaces, *Nat. Mater.* **11**, 103 (2012).
- [5] J. G. Bednorz and K. A. Müller, Perovskite-type oxides—The new approach to high- $T_c$  superconductivity, *Rev. of Mod. Phys.* **60**, 585 (1988).
- [6] K.-I. Kobayashi, T. Kimura, H. Sawada, K. Terakura, and Y. Tokura, Room-temperature magnetoresistance in an oxide material with an ordered double-perovskite structure, *Nature* **395**, 677 (1998).
- [7] J. Wang, J. Neaton, H. Zheng, V. Nagarajan, S. Ogale, B. Liu, D. Viehland, V. Vaithyanathan, D. Schlom, U. Waghmare, *et al.*, Epitaxial BiFeO<sub>3</sub> multiferroic thin film heterostructures, *Science* **299**, 1719 (2003).
- [8] A. Brinkman, M. Huijben, M. Van Zalk, J. Huijben, U. Zeitler, J. Maan, W. G. van der Wiel, G. Rijnders, D. H. Blank, and H. Hilgenkamp, Magnetic effects at the interface between non-magnetic oxides, *Nat. Mater.* **6**, 493 (2007).
- [9] C. Liu, X. Yan, D. Jin, Y. Ma, H.-W. Hsiao, Y. Lin, T. M. Bretz-Sullivan, X. Zhou, J. Pearson, B. Fisher, *et al.*, Two-dimensional superconductivity and anisotropic transport at KTaO<sub>3</sub>(111) interfaces, *Science* **371**, 716 (2021).
- [10] J. A. Bert, B. Kalisky, C. Bell, M. Kim, Y. Hikita, H. Y. Hwang, and K. A. Moler, Direct imaging of the coexistence of ferromagnetism and superconductivity at the LaAlO<sub>3</sub>/SrTiO<sub>3</sub> interface, *Nat. Phys.* **7**, 767 (2011).
- [11] M. C. Tarun, F. A. Selim, and M. D. McCluskey, Persistent photoconductivity in strontium titanate, *Phys. Rev. Lett.* **111**, 187403 (2013).
- [12] Y. Lei, Y. Li, Y. Chen, Y. Xie, Y. Chen, S. Wang, J. Wang, B. Shen, N. Pryds, H. Hwang, *et al.*, Visible-light-enhanced gating effect at the LaAlO<sub>3</sub>/SrTiO<sub>3</sub> interface, *Nat. Commun.* **5**, 5554 (2014).
- [13] Y. Matsubara, K. Takahashi, M. Bahramy, Y. Kozuka, D. Maryenko, J. Falson, A. Tsukazaki, Y. Tokura, and M. Kawasaki, Observation of the quantum Hall effect in  $\delta$ -doped SrTiO<sub>3</sub>, *Nat. Commun.* **7**, 11631 (2016).
- [14] S. Thiel, G. Hammerl, A. Schmehl, C. W. Schneider, and J. Mannhart, Tunable quasi-two-dimensional electron gases in oxide heterostructures, *Science* **313**, 1942 (2006).
- [15] B. Förg, C. Richter, and J. Mannhart, Field-effect devices utilizing LaAlO<sub>3</sub>-SrTiO<sub>3</sub> interfaces, *Appl. Phys. Lett.* **100**, 053506 (2012).
- [16] N. Reyren, S. Thiel, A. review, L. F. Kourkoutis, G. Hammerl, C. Richter, C. W. Schneider, T. Kopp, A.-S. Ruetschi, D. Jaccard, *et al.*, Superconducting interfaces between insulating oxides, *Science* **317**, 1196 (2007).
- [17] A. Caviglia, S. Gariglio, N. Reyren, D. Jaccard, T. Schneider, M. Gabay, S. Thiel, G. Hammerl, J. Mannhart, and J.-M. Triscone, Electric field control of the LaAlO<sub>3</sub>/SrTiO<sub>3</sub> interface ground state, *Nature* **456**, 624 (2008).
- [18] A. Caviglia, M. Gabay, S. Gariglio, N. Reyren, C. Cancellieri, and J.-M. Triscone, Tunable Rashba spin-orbit interaction at oxide interfaces, *Phys. Rev. Lett.* **104**, 126803 (2010).
- [19] A. Caviglia, S. Gariglio, C. Cancellieri, B. Sacépé, A. Fete, N. Reyren, M. Gabay, A. Morpurgo, and J.-M. Triscone, Two-dimensional quantum oscillations of the conductance at LaAlO<sub>3</sub>/SrTiO<sub>3</sub> interfaces, *Phys. Rev. Lett.* **105**, 236802 (2010).
- [20] Y. Chen, J. Zhao, J. Sun, N. Pryds, and B. Shen, Resistance switching at the interface of LaAlO<sub>3</sub>/SrTiO<sub>3</sub>, *Appl. Phys. Lett.* **97**, 123102 (2010).
- [21] S. J. Allen, B. Jalan, S. Lee, D. G. Ouellette, G. Khalsa, J. Jaroszynski, S. Stemmer, and A. H. MacDonald, Conduction-band edge and Shubnikov–de Haas effect in low-electron-density SrTiO<sub>3</sub>, *Phys. Rev. B.* **88**, 045114 (2013).
- [22] N. Wadehra, R. Tomar, R. M. Varma, R. Gopal, Y. Singh, S. Dattagupta, and S. Chakraverty, Planar hall effect and anisotropic magnetoresistance in polar-polar interface of LaVO<sub>3</sub>-KTaO<sub>3</sub> with strong spin-orbit coupling, *Nat. Commun.* **11**, 874 (2020).
- [23] H. M. Christen and G. Eres, Recent advances in pulsed-laser deposition of complex oxides, *Journal of Physics: Condensed Matter* **20**, 264005 (2008).
- [24] A. Ohtomo and H. Hwang, A high-mobility electron gas at the LaAlO<sub>3</sub>/SrTiO<sub>3</sub> heterointerface, *Nature* **427**, 423 (2004).
- [25] N. Nakagawa, H. Y. Hwang, and D. A. Muller, Why some interfaces cannot be sharp, *Nat. Mater.* **5**, 204 (2006).
- [26] Z. S. Popović, S. Satpathy, and R. M. Martin, Origin of the two-dimensional electron gas carrier density at the LaAlO<sub>3</sub> on SrTiO<sub>3</sub> interface, *Phys. Rev. Lett.* **101**, 256801 (2008).
- [27] M. Basletic, J.-L. Maurice, C. Carrétéro, G. Herranz, O. Copie, M. Bibes, É. Jacquet, K. Bouzehouane, S. Fusil, and A. Barthélémy, Mapping the spatial distribution of charge carriers in LaAlO<sub>3</sub>/SrTiO<sub>3</sub> heterostructures, *Nat. Mater.* **7**, 621 (2008).
- [28] J. Heber, Enter the oxides: thin films of oxygen-bearing compounds could have myriad practical applications, finds Joerg Heber, if a few problems can be overcome,

- Nature **459**, 28 (2009).
- [29] R. Ramesh and D. G. Schlom, Whither oxide electronics?, MRS Bulletin **33**, 1006 (2008).
- [30] C. Cen, S. Thiel, J. Mannhart, and J. Levy, Oxide nano-electronics on demand, Science **323**, 1026 (2009).
- [31] J. Eisenstein, K. Cooper, L. Pfeiffer, and K. West, Insulating and fractional quantum hall states in the first excited Landau level, Physical Review Letters **88**, 076801 (2002).
- [32] V. Umansky, M. Heiblum, Y. Levinson, J. Smet, J. Nübler, and M. Dolev, MBE growth of ultra-low disorder 2DEG with mobility exceeding  $35 \times 10^6 \text{ cm}^2/\text{Vs}$ , Journal of Crystal Growth **311**, 1658 (2009).
- [33] S. Stemmer and S. James Allen, Two-dimensional electron gases at complex oxide interfaces, Annu. Rev. Mater. Res. **44**, 151 (2014).
- [34] Z. Zhong, P. Xu, and P. J. Kelly, Polarity-induced oxygen vacancies at  $\text{LaAlO}_3/\text{SrTiO}_3$  interfaces, Phys. Rev. B **82**, 165127 (2010).
- [35] Y. Li, S. N. Phattalung, S. Limpijumnong, J. Kim, and J. Yu, Formation of oxygen vacancies and charge carriers induced in the n-type interface of a  $\text{LaAlO}_3$  overlayer on  $\text{SrTiO}_3(001)$ , Phys. Rev. B **84**, 245307 (2011).
- [36] N. Bristowe, P. Littlewood, and E. Artacho, Surface defects and conduction in polar oxide heterostructures, Phys. Rev. B **83**, 205405 (2011).
- [37] P. Willmott, S. Pauli, R. Herger, C. Schlepütz, D. Martocchia, B. Patterson, B. Delley, R. Clarke, D. Kumah, C. Cionca, *et al.*, Structural basis for the conducting interface between  $\text{LaAlO}_3$  and  $\text{SrTiO}_3$ , Phys. Rev. Lett. **99**, 155502 (2007).
- [38] S. A. Chambers, M. H. Engelhard, V. Shutthanandan, Z. Zhu, T. C. Droubay, L. Qiao, P. Sushko, T. Feng, H. D. Lee, T. Gustafsson, *et al.*, Instability, intermixing and electronic structure at the epitaxial  $\text{LaAlO}_3/\text{SrTiO}_3(001)$  heterojunction, Surf. Sci. Rep. **65**, 317 (2010).
- [39] R. Yamamoto, C. Bell, Y. Hikita, H. Y. Hwang, H. Nakamura, T. Kimura, and Y. Wakabayashi, Structural comparison of n-type and p-type  $\text{LaAlO}_3/\text{SrTiO}_3$  interfaces, Phys. Rev. Lett. **107**, 036104 (2011).
- [40] Y. Chen, F. Trier, T. Kasama, D. V. Christensen, N. Bovet, Z. I. Balogh, H. Li, K. T. S. Thydén, W. Zhang, S. Yazdi, *et al.*, Creation of high mobility two-dimensional electron gases via strain induced polarization at an otherwise nonpolar complex oxide interface, Nano Lett. **15**, 1849 (2015).
- [41] S. Nazir, J. Cheng, and K. Yang, Creating two-dimensional electron gas in nonpolar/nonpolar oxide interface via polarization discontinuity: First-principles analysis of  $\text{CaZrO}_3/\text{SrTiO}_3$  heterostructure, ACS Appl. Mater. Interfaces. **8**, 390 (2016).
- [42] Y. Wang, W. Tang, J. Cheng, M. Behtash, and K. Yang, Creating two-dimensional electron gas in polar/polar perovskite oxide heterostructures: first-principles characterization of  $\text{LaAlO}_3/\text{A}^+\text{B}^{5+}\text{O}_3$ , ACS Appl. Mater. Interfaces. **8**, 13659 (2016).
- [43] L. Fang, C. Chen, Y. Yang, Y. Wu, T. Hu, G. Zhao, Q. Zhu, and W. Ren, First-principles studies of a two-dimensional electron gas at the interface of polar/polar  $\text{LaAlO}_3/\text{KNbO}_3$  superlattices, Phys. Chem. Chem. Phys. **21**, 8046 (2019).
- [44] K. Zou, S. Ismail-Beigi, K. Kisslinger, X. Shen, D. Su, F. Walker, and C. Ahn,  $\text{LaTiO}_3/\text{KTaO}_3$  interfaces: A new two-dimensional electron gas system, APL Mater. **3**, 036104 (2015).
- [45] Y. Xie, Y. Hikita, C. Bell, and H. Y. Hwang, Control of electronic conduction at an oxide heterointerface using surface polar adsorbates, Nat. Commun. **2**, 494 (2011).
- [46] I. Pallecchi, M. Codda, E. G. d'Agliano, D. Marré, A. Reivew, N. Reyren, S. Gariglio, and J.-M. Triscone, Seebeck effect in the conducting  $\text{LaAlO}_3/\text{SrTiO}_3$  interface, Phys. Rev. B. **81**, 085414 (2010).
- [47] A. Filippetti, P. Delugas, M. Verstraete, I. Pallecchi, A. Gadaleta, D. Marré, D. Li, S. Gariglio, and V. Fiorentini, Thermopower in oxide heterostructures: The importance of being multiple-band conductors, Phys. Rev. B. **86**, 195301 (2012).
- [48] E. Assmann, P. Blaha, R. Laskowski, K. Held, S. Okamoto, and G. Sangiovanni, Oxide heterostructures for efficient solar cells, Phys. Rev. Lett. **110**, 078701 (2013).
- [49] H. Liang, L. Cheng, X. Zhai, N. Pan, H. Guo, J. Zhao, H. Zhang, L. Li, X. Zhang, X. Wang, *et al.*, Giant photovoltaic effects driven by residual polar field within unit-cell-scale  $\text{LaAlO}_3$  films on  $\text{SrTiO}_3$ , Sci. Rep. **3**, 1975 (2013).
- [50] P. Irvin, Y. Ma, D. F. Bogorin, C. Cen, C. W. Bark, C. M. Folkman, C.-B. Eom, and J. Levy, Rewritable nanoscale oxide photodetector, Nat. Photon. **4**, 849 (2010).
- [51] A. Tebano, E. Fabbri, D. Pergolesi, G. Balestrino, and E. Traversa, Room-temperature giant persistent photoconductivity in  $\text{SrTiO}_3/\text{LaAlO}_3$  heterostructures, ACS Nano **6**, 1278 (2012).
- [52] A. Rastogi, A. Kushwaha, T. Shiyani, A. Gangawar, and R. Budhani, Electrically tunable optical switching of a mott insulator–band insulator interface, Adv. Mater. **22**, 4448 (2010).
- [53] H.-L. Lu, Z.-M. Liao, L. Zhang, W.-T. Yuan, Y. Wang, X.-M. Ma, and D.-P. Yu, Reversible insulator-metal transition of  $\text{LaAlO}_3/\text{SrTiO}_3$  interface for nonvolatile memory, Sci. Rep. **3**, 2870 (2013).
- [54] N. Kumar, N. Wadehra, R. Tomar, S. Dattagupta, S. Kumar, and S. Chakraverty, Observation of Shubnikov-de Haas Oscillations, Non-trivial Berry Phase, Planar Hall and Anisotropic Magnetoresistance at the conducting interface of  $\text{EuO-KTaO}_3$ , arXiv preprint arXiv:1908.04977 (2019).
- [55] N. Wadehra and S. Chakraverty, Electrostatic memory in  $\text{KTaO}_3$ , Appl. Phys. Lett. **114** (2019).
- [56] S. Goyal, N. Wadehra, and S. Chakraverty, Tuning the electrical state of 2DEG at  $\text{LaVO}_3 - \text{KTaO}_3$  interface: effect of light and electrostatic gate, Adv. Mater. Interfaces **7**, 2000646 (2020).
- [57] P. Giannozzi, S. Baroni, N. Bonini, M. Calandra, R. Car, C. Cavazzoni, D. Ceresoli, G. L. Chiarotti, M. Cococcioni, I. Dabo, A. D. Corso, S. de Gironcoli, S. Fabris, G. Fratesi, R. Gebauer, U. Gerstmann, C. Gougoussis, A. Kokalj, M. Lazzeri, L. Martin-Samos, N. Marzari, F. Mauri, R. Mazzarello, S. Paolini, A. Pasquarello, L. Paulatto, C. Sbraccia, S. Scandolo, G. Sclauzero, A. P. Seitsonen, A. Smogunov, P. Umari, and R. M. Wentzcovitch, QUANTUM ESPRESSO: a modular and open-source software project for quantum simulations of materials, J. Phys.: Condens. Matter **21**, 395502 (2009).
- [58] D. Vanderbilt, Soft self-consistent pseudopotentials in a generalized eigenvalue formalism, Phys. Rev. B **41**, 7892 (1990).

- [59] J. P. Perdew, K. Burke, and M. Ernzerhof, Generalized gradient approximation made simple, *Phys. Rev. Lett.* **77**, 3865 (1996).
- [60] M. Cococcioni and S. De Gironcoli, Linear response approach to the calculation of the effective interaction parameters in the LDA +  $U$  method, *Phys. Rev. B* **71**, 035105 (2005).
- [61] A. Liechtenstein, V. I. Anisimov, and J. Zaanen, Density-functional theory and strong interactions: Orbital ordering in mott-hubbard insulators, *Physical Review B* **52**, R5467 (1995).
- [62] L. Wang, Y. Li, A. Bera, C. Ma, F. Jin, K. Yuan, W. Yin, A. David, W. Chen, W. Wu, *et al.*, Device performance of the mott insulator  $\text{LaVO}_3$  as a photovoltaic material, *Physical Review Applied* **3**, 064015 (2015).
- [63] V. R. Cooper, Enhanced carrier mobilities in two-dimensional electron gases at III-III/IV oxide heterostructure interfaces, *Physical Review B—Condensed Matter and Materials Physics* **85**, 235109 (2012).
- [64] H. J. Monkhorst and J. D. Pack, Special points for Brillouin-zone integrations, *Phys. Rev. B* **13**, 5188 (1976).
- [65] N. Marzari, D. Vanderbilt, A. De Vita, and M. C. Payne, Thermal contraction and disordering of the Al(110) surface, *Phys. Rev. Lett.* **82**, 3296 (1999).
- [66] S. Y. Park, A. Kumar, and K. M. Rabe, Charge-order-induced ferroelectricity in  $\text{LaVO}_3/\text{SrVO}_3$  superlattices, *Physical review letters* **118**, 087602 (2017).
- [67] P. Bordet, C. Chaillout, M. Marezio, Q. Huang, A. Santoro, S. Cheong, H. Takagi, C. Oglesby, and B. Batlogg, Structural aspects of the crystallographic-magnetic transition in  $\text{LaVO}_3$  around 140 K, *Journal of solid state chemistry* **106**, 253 (1993).
- [68] H. Bouafia, S. Hiadsi, B. Abidri, A. Akriche, L. Ghalouci, and B. Sahli, Structural, elastic, electronic and thermodynamic properties of  $\text{KTaO}_3$  and  $\text{NaTaO}_3$ : Ab initio investigations, *Computational materials science* **75**, 1 (2013).
- [69] S. Wemple, Some transport properties of oxygen-deficient single-crystal potassium tantalate ( $\text{KTaO}_3$ ), *Physical Review* **137**, A1575 (1965).
- [70] B. Rechav, Y. Yacoby, E. Stern, J. Rehr, and M. Newville, Order disorder elements in antiferrodistortive phase transitions, *Physica B: Condensed Matter* **208**, 325 (1995).
- [71] M. De Raychaudhury, E. Pavarini, and O. Andersen, Orbital fluctuations in the different phases of  $\text{LaVO}_3$  and  $\text{YVO}_3$ , *Physical review letters* **99**, 126402 (2007).
- [72] S. Kumari, S. Paul, and S. Raj, Electronic structure of  $\text{RVO}_3$  ( $R = \text{La}$  and  $\text{Y}$ ): Effect of electron ( $U$ ) and exchange ( $J$ ) correlations, *Solid State Commun.* **268**, 20 (2017).
- [73] G. Jellison Jr, I. Paulauskas, L. Boatner, and D. Singh, Optical functions of  $\text{KTaO}_3$  as determined by spectroscopic ellipsometry and comparison with band structure calculations, *Phys. Rev. B* **74**, 155130 (2006).
- [74] S. Kakkar and C. Bera, Rashba spin splitting in two-dimensional electron gas in polar-polar perovskite oxide heterostructure  $\text{LaVO}_3/\text{KTaO}_3$ : A DFT investigation, *Physica E: Low-dimensional Systems and Nanostructures* **144**, 115394 (2022).
- [75] S. Okamoto, A. J. Millis, and N. A. Spaldin, Lattice relaxation in oxide heterostructures:  $\text{LaTiO}_3/\text{SrTiO}_3$  superlattices, *Physical review letters* **97**, 056802 (2006).
- [76] S. Ryu, H. Zhou, T. Paudel, J. Irwin, J. Podkaminer, C. Bark, D. Lee, T. Kim, D. Fong, M. Rzchowski, *et al.*, In-situ probing of coupled atomic restructuring and metallicity of oxide heterointerfaces induced by polar adsorbates, *Applied Physics Letters* **111** (2017).
- [77] T. R. Paudel and E. Y. Tsymbal, Prediction of a mobile two-dimensional electron gas at the  $\text{LaScO}_3/\text{BaSnO}_3(001)$  interface, *Physical Review B* **96**, 245423 (2017).
- [78] S. Patel, N. Mohanta, S. Nandy, S. D. Mahanti, and A. Taraphder, Layer-dependent electronic structures and magnetic ground states of polar-polar  $\text{LaVO}_3/\text{KTaO}_3(001)$  heterostructures, *Physical Review B* **110**, 054402 (2024).
- [79] Z. Zhong, A. Tóth, and K. Held, Theory of spin-orbit coupling at  $\text{LaAlO}_3/\text{SrTiO}_3$  interfaces and  $\text{SrTiO}_3$  surfaces, *Physical Review B—Condensed Matter and Materials Physics* **87**, 161102 (2013).
- [80] M. Behtash, S. Nazir, Y. Wang, and K. Yang, Polarization effects on the interfacial conductivity in  $\text{LaAlO}_3/\text{SrTiO}_3$  heterostructures: A first-principles study, *Physical Chemistry Chemical Physics* **18**, 6831 (2016).
- [81] Y. Wang, M. K. Niranjana, J. D. Burton, J. M. An, K. D. Belashchenko, and E. Y. Tsymbal, Prediction of a spin-polarized two-dimensional electron gas at the  $\text{LaAlO}_3/\text{EuO}(001)$  interface, *Physical Review B—Condensed Matter and Materials Physics* **79**, 212408 (2009).
- [82] S. Nazir and K. Yang, First-principles characterization of the critical thickness for forming metallic states in strained  $\text{LaAlO}_3/\text{SrTiO}_3(001)$  heterostructure, *ACS Applied Materials & Interfaces* **6**, 22351 (2014).